In vitro and Numerical Simulation of Blood Removal from Cerebrospinal Fluid: Comparison of Lumbar Drain to Neurapheresis Therapy

Mohammadreza Khani
University of Idaho
Lucas Sass
University of Idaho
M. Keith Sharp
University of Louisville
Aaron McCabe
minnetronix medical
Laura Zitella Verbick
minnetronix medical
Shivanand Lad
Duke University
bryn martin (brynm@uidaho.edu)
https://orcid.org/0000-0003-1234-7880

Research

Keywords: Computational fluid dynamics, In-vitro model, Subarachnoid hemorrhage, Neurapheresis therapy, Cerebrospinal fluid filtration, Multiphase simulation.

Posted Date: March 10th, 2020

DOI: https://doi.org/10.21203/rs.2.20844/v3

Version of Record: A version of this preprint was published at Fluids and Barriers of the CNS on March 16th, 2020. See the published version at https://doi.org/10.1186/s12987-020-00185-5.

Abstract

Background: Blood removal from cerebrospinal fluid (CSF) in post-subarachnoid hemorrhage patients may reduce the risk of related secondary brain injury. We formulated a computational fluid dynamics (CFD) model to investigate the impact of a dual-lumen catheter-based CSF filtration system, called Neurapheresis^{TM} therapy, on blood removal from CSF compared to lumbar drain.

Methods: A subject-specific multiphase CFD model of CSF system-wide solute transport was constructed based on MRI measurements. The Neurapheresis catheter geometry was added to the model within the spinal subarachnoid space (SAS). Neurapheresis flow aspiration and return rate was 2.0 and 1.8 mL/min, versus 0.2 mL/min drainage for lumbar drain. Blood was modeled as a bulk fluid phase within CSF with a 10% initial tracer concentration and identical viscosity and density as CSF. Subject-specific oscillatory CSF flow was applied at the model inlet. The dura and spinal cord geometry were considered to be stationary. Spatial-temporal tracer concentration was quantified based on time-average steady-streaming velocities throughout the domain under Neurapheresis therapy and lumbar drain. To help verify CFD results, an optically clear in vitro CSF model was constructed with fluorescein used as a blood surrogate. Quantitative comparison of numerical and in vitro results was performed by linear regression of spatial-temporal tracer concentration over 24-hours.

Results: After 24-hours, tracer concentration was reduced to 4.9% under Neurapheresis therapy compared to 6.5% under lumbar drain. Tracer clearance was most rapid between the catheter aspiration and return ports. Neurapheresis therapy was found to have a greater impact on steady-streaming compared to lumbar drain. Steady-streaming in the cranial SAS was ~50X smaller than in the spinal SAS for both cases. CFD results were strongly correlated with the in vitro spatial-temporal tracer concentration under Neurapheresis therapy (R^2=0.89 with +2.13% and -1.93% tracer concentration confidence interval).

Conclusion: A subject-specific CFD model of CSF system-wide solute transport was used to investigate the impact of Neurapheresis therapy on tracer removal from CSF compared to lumbar drain over a 24-hour period. Neurapheresis therapy was found to substantially increase tracer clearance compared to lumbar drain. The multiphase CFD results were verified by in vitro fluorescein tracer experiments.

Background

A detailed understanding of cerebrospinal fluid (CSF) physiologic function may help improve treatment of CSF-related central nervous system (CNS) diseases and debilitating neurological conditions. CSF is a clear, colorless fluid that occupies the subarachnoid space (SAS) and the ventricular system within the brain (1). CSF is believed to be primarily produced within the ventricles of the brain by secretory epithelial cells which form the choroid plexuses and absorbed at the arachnoid granulations located in the SAS on the surface of the superior sagittal sinus (2). CSF moves with a net flow direction outward from the ventricles to the SAS but also multi-directionally with an oscillatory motion, driven by cardiac and respiratory-related pressure fluctuations and other transient maneuvers (3). CSF serves multiple

physiological functions that continue to be discovered. Some of the roles of CSF include: 1) suspension of the delicate brain tissue by the Archimedes principle making the brain tissue nearly neutrally buoyant, 2) damping of forces that act on the brain tissue due to transient impact (4), 3) providing immunological and biochemical homeostasis for the CNS (5), and 4) delivery of metabolites and micronutrients to the CNS (1, 6).

The importance of CSF dynamics has been investigated in several CNS diseases that include neuroinflammatory conditions such as multiple sclerosis (7, 8) and neurovascular conditions such as cerebral ischemia (9, 10), traumatic brain injury (11) and subarachnoid hemorrhage (SAH) (12). Delayed ischemia and hydrocephalus following SAH are two of the primary causes of morbidity/mortality due to the presence of blood in the subarachnoid spaces (SAS) (13-15). Therefore, strategies to facilitate the rapid clearance of blood from the SAS may reduce the risk of these complications to patients. Such strategies, including lumbar drain (12, 16), cisternal drainage (17, 18) and cisternal lavages (19, 20), have been studied by a number of investigators, but the exact biological mechanisms responsible for delayed ischemia are not yet clear.

Neurapheresis^{TM} therapy (Minnetronix Neuro, Inc., St. Paul, MN) is being investigated as a means to potentially rapidly remove red blood cells from the SAS and consequently decrease the incidence or severity of secondary complications. In brief, Neurapheresis therapy involves aspiration of CSF from the lumbar spinal SAS, filtration of CSF and removal of red blood cells and detritus to a waste bag, and then return of filtered CSF to the SAS at the thoracic spine. The different locations of the aspiration and return ports may facilitate advective bulk movement of CSF between the ports within the SAS. Additional details on Neurapheresis therapy are provided by Khani et al.(21).

Computational and in vitro modeling constitute potential methods to study complex transport phenomena occurring during blood clearance from CSF spaces and, subsequently, to improve devices and protocols to treat neural disorders. Clinical trials to develop guidelines for more effective clearance are difficult due to limited availability of subjects and associated study costs. Empirical models limit our ability to investigate CSF filtration technologies, highlighting the need for a computational tool. Human clinical trials of Neurapheresis therapy in SAH patients are being conducted (PILLAR trial (22-24)), but these studies lack real-time visualization of blood distribution and are only able to sample CSF from select locations. Real-time visualization is important in this study because it helps us to monitor the tracer concentration at each location and time frame and then use it to predict the total the time needed to completely remove all the blood from CSF system for a subject-specific patient. Results from this real-time visualization could be used to estimate and compare the efficiency of the Neurapheresis therapy to traditional lumbar drain at each time point. Also, in principle, a nonhuman primate experimental model of SAH could be developed, but such studies are expensive, are only available at limited research centers, and do not provide similar CSF dynamics to humans (25, 26).

Several in vivo, in vitro, and in silico studies have been conducted to better understand Neurapheresis therapy. A rabbit model was used to investigate Neurapheresis therapy in the context of cryptococcal

meningitis. This study showed a 5-log reduction in yeast concentration and 1-log reduction in its polysaccharide antigen over 24-hours. A drawback of the study was that the rabbit model has an extremely small SAS, thus it is unclear how rabbit CSF dynamics compare to humans (27). A study by Tangen et al. (28) presented a computational and in vitro model of SAH clearance from CSF. This study provided information about the potential of CSF filtration to assist with blood removal under different body orientations (i.e., supine versus upright) with an idealized representation of CSF space anatomy. Khani et al. formulated a numerical model to investigate the impact of Neurapheresis therapy on CSF flow velocities in a realistic spinal SAS geometry with subject-specific CSF flow along the spine (21). However, this model did not take into account the intracranial portion of the CSF system and lacked a multiphase fluid mixture of blood and CSF.

While the previous studies provided insight into Neurapheresis therapy, they had the following important limitations: a) they lacked realistic system-wide CSF geometry, b) they did not consider the multi-phase solute transport within the CSF, c) they were conducted over relatively short time periods, d) they utilized animal models that have different CSF dynamics than humans, and/or e) they lacked numerical model solution verification. This study seeks to address these limitations by formulating a multi-phase numerical model of CSF system-wide solute transport within an anatomically realistic human geometry and by verifying the numerical solution versus in vitro measurements.

Methods

Due to technical limitations, the Methods section is only available as a download in the supplemental files section.

Results

Due to technical limitations, the Results section is only available as a download in the supplemental files section.

Discussion

The CFD and in vitro model provided a systematic comparison of lumbar drain to Neurapheresis therapy after SAH. These models allow detailed comparison of results without the confounding impact of many variables that would be difficult to control for in vivo animal models or SAH patients. Computer simulations provided the theoretical basis to interpret bench top in vitro results by better elucidating the complex tracer clearance patterns in pulsatile CSF after SAH.

In vitro verification of numerical results

Studies show that wide variability exists in CFD modeling techniques and the choice of numerical solvers and settings are complex and can yield disparate results for biofluids simulations (53). Thus, in vitro models play a critical role to help verify numerical results. Unfortunately, at present there is no known

method to map exact spatial-temporal blood concentration within the CSF over time for SAH patients. Thus, a true model validation against in vivo measurements is not possible. The model results are presented as a prediction for how blood can potentially be removed from the CSF.

Comparison of spatial-temporal cross-sectional average tracer concentration profiles revealed similar clearance trends for both CFD and in vitro under Neurapheresis therapy and lumbar drain conditions (**Fig 5**). A strong linear correlation was found between CFD and in vitro results under Neurapheresis therapy (R^2=0.89, **Fig 7a1**), and a moderate linear correlation for lumbar drain (R^2 = 0.65, **Fig 7b1**). Lumbar drain correlation was lower likely due to the lower degree of tracer changes that were present in that experiment. It was noted that linear correlation of results was stronger within the central region of the models. We expect that results had improved agreement within the central region of the model because our optical imaging field of view was most accurately aligned to CFD results within that region of the model. Near the model ends, the camera viewing angle was not orthogonal to the model domain and therefore did not provide information in the exact axial z-orientation as CFD results. Even with these in vitro imaging limitations, CFD results showed 95% of the CFD tracer concentration results were within ~2% of the in vitro findings with a mean difference of ~0.1% in both cases (**Fig 7a2** and **b2**). In combination, these results help verify the numerical modeling approach using a frozen flow field that excluded mass diffusion. While these results agree, they cannot be assumed to correctly represent in vivo as many model assumptions were made that may not exactly represent in vivo CSF mass transport (see limitations). These model predictions should be tested against in vivo measurements in animals and/or humans.

Our model results are difficult to directly compare with previous research as no study has been conducted previously with an anatomically realistic model and with Neurapheresis therapy applied with an exact catheter geometry. However, Tangen et al (37) used an anatomically idealized bench-top CSF model and corresponding CFD analysis to study CSF blood clearance following SAH under various body orientations and lumbar drain rates with an intraventricular catheter inserted for 3 hours. They found the fastest blood clearance was achieved in the vertical body position and that an increase in lumbar drainage flow rate accelerated blood clearance. Their results, using a lumbar drain and intraventricular catheter, showed that after 60 minutes of filtration, contamination concentration was 3.5% at the T6 vertebral level. After 60 minutes, tracer clearance was 1.5 % at T6 in our numerical model using Neurapheresis therapy (**Fig 5a1**). This difference is likely due to the 2X higher filtration rate applied in our study 2.0 mL/min versus 1.0 mL/min by Tangen et al. Also, for the lumbar drain case with 0.2 mL/min drainage rate, 12% clearance was observed in Tangen et al (37) versus 10% clearance in our simulation. Since drainage rate for lumbar drain is equal on both studies, the clearance rates are similar.

Comparison of Neurapheresis therapy and lumbar drain

After 24 hours, results from Neurapheresis therapy showed that 4.9% of tracer remained in the model (**Fig 6a**) while 6.5% tracer concentration remained after lumbar drainage (**Fig 6b)**. Cranial tracer clearance was nearly identical in both the lumbar drain and Neurapheresis therapy (**Fig 5a1** and **5b1**). The mechanistic

reason for increased tracer clearance under Neurapheresis therapy is that it applies a CSF flow loop that returns filtered CSF back to the upper thoracic spine. The CSF flow loop increases steady-streaming velocities within the flow loop region (**Fig. 4**), which allows more rapid removal of the tracer. While the clinical impact of greater blood clearance on SAH outcomes has not been proven, researchers have shown the potential that more quickly reducing the levels of blood and inflammatory cytokines in the CSF post SAH could improve outcomes (54, 55)

The Neurapheresis therapy flow rate applied in our study was 2.0 mL/min with a 1.8 mL/min return flow rate. A flow rate of 2.0 mL/min is not possible to apply using a lumbar drain because it would remove CSF more rapidly than it is being produced at the choroid plexus (~500 mL/day) (56). To help compare Neurapheresis and lumbar drain tracer clearance efficiency, we compared tracer clearance under a lumbar drain and Neurapheresis waste rate both set to 0.2 mL/min (288 mL in 24 hours). To the best of our knowledge, this flow rate represents an upper bound for what is possible to withdraw under lumbar drain. In clinical practice, the drainage rate settings for lumbar drains may be lower.

Importance of frozen field approach in the numerical model

Transient simulations of oscillating fluids are computationally intensive, in particular when conducted over long time periods with small time-step size. For example, in the present case representing CSF oscillations, computation of a single CSF flow cycle requires ~3.6 hours using 38 processors (Intel(R) Xeon(R) Gold 6148 CPU @ 2.40GHz) and 126 (GB) Memory. Simultaneously solving the passive transport equation requires additional time. Neurapheresis therapy is conducted over a period of more than 24-hours. As such, we applied a two-part CFD method that neglected diffusion to obtain a computationally tractable solution over the 24-hour timeframe. First, a transient Navier-Stokes solution of 11 flow cycles was performed to obtain the steady-streaming velocity field. Steady-streaming is postulated to be responsible for the time-average bulk movement of CSF in the SAS that results from nonlinear cumulative effects of convective acceleration (57). Steady streaming is important in this context because it has been shown to be the primary mode of mass transport within the oscillatory CSF flow field (58). Second, the velocity field was applied as a “frozen flow field” as described by Kuttler et al.(40). The frozen field approach is valid for periodic flow when advection is the main mode of mass transport.

The numbers computed in our study, by using the effective diffusivity of the tracer, were 7.56 E-06 and 9.6 E-03 for the cortical and spinal SAS, respectively. It should be noted that the low Sherwood number based on does not necessarily convey that shear-augmented diffusion is important, in particular for the present case in which substantial mixing can be produced by the complex spinal cord nerve root geometry. Further study is needed to compare the effect of diffusion to steady-streaming based advection.

In this study, we did not include the potential impact of microscopic anatomy within the domain such as arachnoid trabeculae or blood vessels, nor hydrodynamic affects on finite-size particles (red blood cells, in particular). Other numerical studies have investigated the potential impact of microscopic structures (41) within the CSF and found they can have varying degrees of impact on solute transport (59-61) and pressure gradients (62). Thus, our numerical and in vitro predictions should be confirmed with in vivo

experiments. Albeit, these experiments may not be possible at present as we do not have a non-invasive in vivo imaging modality that can quantify blood concentration throughout the CSF system over 24-hours.

Limitations

In this study, blood dispersion was modeled by fluorescein tracer mixed in a single continuum CSF phase at room temperature. Physiologically, blood cells and debris create a suspension when mixed into CSF. The biochemistry of blood coagulation within the CSF was not reproduced. Additionally, once exposed to the SAS environment, blood cells can rupture releasing oxyhemoglobin which is further enzymatically converted to bilirubin (63, 64). While the electrolytes and enzymatic interactions between blood components and CSF have an impact, our fluid mechanical study did not take into account pharmacokinetics of blood proteins, blood cell lysis, and blood cell component metabolism. Accounting for red blood cell byproducts and reaction kinetics could provide a more realistic scenario for testing biochemical effects of SAH. However, the effective diffusivity is independent of molecular diffusivity since R_{max} is large compared to unity. Therefore, the chosen tracer provides good similitude for blood. The in vitro experiments were performed at 19 ºC. We did not create a thermostatic environment due to size limitations, because the density ratio between CSF and fluorescein tracer is not different whether the experiment is conducted at 19 ºC or at body temperature of 37 ºC.

In the comparison between simulation and experiments, the highest deviations occurred in the cranial SAS. It is likely these differences were larger in the cranial SAS due to the 2D imaging technique that used a picture obtained for a single angle relative to the model, whereas, the CFD concentrations were precisely averaged across each 3 mm thick slice, including fluid located within the ventricles of the brain. Future work could potentially improve agreement of in vitro and numerical results by utilizing tomographic projection imaging (65) of the in vitro model or quantitative contrast enhanced MRI techniques (66).

The numerical simulations in this study were based on MRI measurements for a single subject-specific CSF system geometry and CSF flow waveform. These parameters should be investigated in a larger cohort to determine the potential impact of age, sex, and disease states on CSF solute transport. However, the consistency of CSF dynamics across humans in the healthy state and with ALS has been studied by our group and we found relatively small differences across subjects (67). Therefore, we expect our results would hold true for other human cases with slightly different CSF space geometry. Also, for future research, we may need to investigate the effect of filtration for a longer periods of 48, 72 or 120 hours for different neurological conditions (68).

Our modeling approach did not include flow oscillations within the ventricles (69, 70) or a respiratory component of CSF pulsations (71-73) because the MRI scanning time did not allow measurement of these parameters in addition to the other parameters used to formulate the model. Additionally, the presented model used a rigid material in which boundary motion of the dura was not prescribed (25). This model also did not account for permeability of the CNS tissue or dura matter (74). We chose a rigid

model without permeability to allow verification of numerical results in a precisely known domain. Future studies should investigate the relevance of tissue permeability and motion.

Our model only had one single site of CSF production in the lateral ventricles because the focus of our study was on CSF solute transport within the subarachnoid space, external to the ventricles, we simplified CSF production to occur at a single site within the lateral ventricle. CSF production was assumed to flow out into the cisterna magna where mixing occurs with CSF in the subarachnoid space. Also, the in vitro system did not allow imaging of tracer concentration within the ventricles, and therefore we were not able to compare in vitro to computational results within the ventricles. Future studies should investigate the impact of CSF production location by adding the choroid plexus in the third and fourth ventricles.

No attempt was made in this study to optimize catheter design or positioning for Neurapheresis therapy. The effect of Neurapheresis therapy on CSF steady-streaming velocities in the spinal SAS were investigated in our previous study (21). The present study extended the previous model by including a complete CSF system, integration of a two-phase model, and developing a method for in vitro verification of results.

Conclusion

A subject-specific CFD model of the CSF system was formulated and applied to compare the impact of Neurapheresis therapy on tracer removal from CSF compared to lumbar drain over a 24-hour period. Results were verified with an in vitro model built identical to the CFD model. The numerical modeling approach using a frozen flow field to represent solute transport resulted in similar solute transport dynamics as that seen in vitro. Using the verified computational model with in vitro system, the results predict that Neurapheresis therapy significantly increases tracer clearance compared to a lumbar drain. The overall tracer concentration after a 24-hour period for Neurapheresis therapy was 4.9% compared to 6.5% with lumbar drain. This effect was maximized within the region between the return and the aspiration ports in Neurapheresis therapy.

Declaration

Ethics approval and consent to participate

In this study, all the MRI data collection development was approved by the local institutional review board in Amiens, France and satisfied all local and international regulations for human subject research. All data was de-identified before transferring to the University of Idaho for further analysis.

Consent for publication

All authors have approved the manuscript submission. The content of this manuscript has not been published or submitted for publication elsewhere.

Availability of data and material

The data that support the findings of this study are available from the corresponding author, [BAM], upon reasonable request.

Competing interests

BAM has received research funding from Biogen Inc., KBR Wyle, Alcyone Lifesciences Inc., Minnetronix Inc., and Voyager Therapeutics.

Funding

This work was supported by Minnetronix Corp., an Institutional Development Award (IDeA) from the National Institute of General Medical Sciences (NIGMS) of the National Institutes of health (NIH) under Grant #P20GM1033408 and #4U54GM104944-04TBD, The National Institute of Mental Health Grant #1R44MH112210-01A1, National Institute of Neurological Disorders and Stroke Grant# R01NS111283, and University of Idaho Vandal Ideas Project.

Author contributions

Study conception and design: BAM, MK

Acquisition of data: MK, LRS

Analysis and interpretation of data: MK, BAM, LRS

Drafting of manuscript: MK, BAM

Critical revision: BAM, MKS, AM, LZV, SPL

Acknowledgments

None.

Abbreviations

P	Density (Kg m^{-3})
M	Dynamic viscosity (Pa s)
N	Kinematic viscosity (m^2 s^{-1})
A	Volume fraction
A	Area
D	Diffusion coefficient
H	Convective mass transport
I	Signal intensity
L	Characteristic length
Q	Flow rate
U	Velocity
V	Cell volume
D_H	Hydraulic diameter
Re	Reynolds number
Sc	Schmidt number
Sh	Sherwood number
CFD	Computational fluid dynamics
CNS	Central nervous system
CSF	Cerebrospinal fluid
MRI	Magnetic resonance imaging
SAH	Subarachnoid hemorrhage
SAS	Subarachnoid spaces

References

1. Wright BL, Lai JT, Sinclair AJ. Cerebrospinal fluid and lumbar puncture: a practical review. J Neurol. 2012;259(8):1530-45. Epub 2012/01/27.
2. Del Bigio MR. Ependymal cells: biology and pathology. Acta Neuropathol. 2010;119(1):55-73.
3. Sakka L, Coll G, Chazal J. Anatomy and physiology of cerebrospinal fluid. Eur Ann Otorhinolaryngol Head Neck Dis. 2011;128(6):309-16. Epub 2011/11/22.

4. Brodbelt A, Stoodley M. CSF pathways: a review. Br J Neurosurg. 2007;21(5):510-20. Epub 2007/10/09.
5. Engelhardt B, Coisne C. Fluids and barriers of the CNS establish immune privilege by confining immune surveillance to a two-walled castle moat surrounding the CNS castle. Fluids Barriers CNS. 2011;8(1):4. Epub 2011/02/26.
6. Spector R, Robert Snodgrass S, Johanson CE. A balanced view of the cerebrospinal fluid composition and functions: Focus on adult humans. Exp Neurol. 2015;273:57-68. Epub 2015/08/08.
7. Freedman MS, Thompson EJ, Deisenhammer F, Giovannoni G, Grimsley G, Keir G, et al. Recommended standard of cerebrospinal fluid analysis in the diagnosis of multiple sclerosis: a consensus statement. Arch Neurol. 2005;62(6):865-70.
8. Hatterer E, Touret M, Belin MF, Honnorat J, Nataf S. Cerebrospinal fluid dendritic cells infiltrate the brain parenchyma and target the cervical lymph nodes under neuroinflammatory conditions. Plos One. 2008;3(10):e3321.
9. Simon MJ, Iliff JJ. Regulation of cerebrospinal fluid (CSF) flow in neurodegenerative, neurovascular and neuroinflammatory disease. Biochim Biophys Acta. 2016;1862(3):442-51.
10. Hardemark HG, Persson L, Bolander HG, Hillered L, Olsson Y, Pahlman S. Neuron-Specific Enolase Is a Marker of Cerebral-Ischemia and Infarct Size in Rat Cerebrospinal-Fluid. Stroke. 1988;19(9):1140-4.
11. Zetterberg H, Smith DH, Blennow K. Biomarkers of mild traumatic brain injury in cerebrospinal fluid and blood. Nat Rev Neurol. 2013;9(4):201-10.
12. Klimo P, Jr., Kestle JR, MacDonald JD, Schmidt RH. Marked reduction of cerebral vasospasm with lumbar drainage of cerebrospinal fluid after subarachnoid hemorrhage. J Neurosurg. 2004;100(2):215-24.
13. Macdonald RL. Pathophysiology and molecular genetics of vasospasm. Cerebral Vasospasm. 2001;77:7-11.
14. Weir B, Macdonald RL, Stoodley M. Etiology of cerebral vasospasm. Acta Neurochir Suppl. 1999;72:27-46.
15. Prim Capdevila J, Campillo Valero D, Coello Gomez F. [Hydrocephalus after subarachnoid hemorrhage]. Neurologia. 1990;5(2):41-4. Epub 1990/02/01. Hidrocefalia posthemorragia subaracnoidea.
16. Hoekema D, Schmidt RH, Ross I. Lumbar drainage for subarachnoid hemorrhage: technical considerations and safety analysis. Neurocrit Care. 2007;7(1):3-9.
17. Inagawa T, Kamiya K, Matsuda Y. Effect of continuous cisternal drainage on cerebral vasospasm. Acta Neurochir (Wien). 1991;112(1-2):28-36.
18. Kawamoto S, Tsutsumi K, Yoshikawa G, Shinozaki MH, Yako K, Nagata K, et al. Effectiveness of the head-shaking method combined with cisternal irrigation with urokinase in preventing cerebral vasospasm after subarachnoid hemorrhage. J Neurosurg. 2004;100(2):236-43.

19. Nakagomi T, Takagi K, Narita K, Nagashima H, Tamura A. Cisternal washing therapy for the prevention of cerebral vasospasm following aneurysmal subarachnoid hemorrhage. Acta Neurochir Suppl. 2001;77:161-5.
20. Sasaki T, Kodama N, Kawakami M, Sato M, Asari J, Sakurai Y, et al. Urokinase cisternal irrigation therapy for prevention of symptomatic vasospasm after aneurysmal subarachnoid hemorrhage: a study of urokinase concentration and the fibrinolytic system. Stroke. 2000;31(6):1256-62.
21. Khani M, Sass L, McCabe A, Zitella Verbick L, Lad SP, Sharp MK, et al. Impact of Neurapheresis system on intrathecal cerebrospinal fluid dynamics: a computational fluid dynamics study. J Biomech Eng. 2019. Epub 2019/07/26.
22. Blackburn SL, Swisher CB, Grande AW, Rubi A, Verbick LZ, McCabe A, et al. Novel Dual Lumen Catheter and Filtration Device for Removal of Subarachnoid hemorrhage: First Case Report. Oper Neurosurg (Hagerstown). 2018.
23. Extracorporeal Filtration of Subarachnoid Hemorrhage Via Spinal Catheter (PILLAR). 2018 [cited 2018 11/9/2018]; Available from: https://clinicaltrials.gov/ct2/show/NCT02872636?term=pillar&cond=Subarachnoid+Hemorrhage&rank=1.
24. Blackburn SL, Grande AW, Swisher CB, Hauck EF, Jagadeesan B, Provencio JJ. Prospective Trial of Cerebrospinal Fluid Filtration After Aneurysmal Subarachnoid Hemorrhage via Lumbar Catheter (PILLAR). Stroke. 2019;50(9):2558-61. Epub 2019/07/28.
25. Khani M, Sass L, Xing T, Sharp MK, Balédent O, Martin B. Anthropomorphic Model of Intrathecal Cerebrospinal Fluid Dynamics Within the Spinal Subarachnoid Space: Spinal Cord Nerve Roots Increase Steady-Streaming. Journal of Biomechanical Engineering. 2018.
26. Khani M, Lawrence BJ, Sass LR, Gibbs CP, Pluid JJ, Oshinski JN, et al. Characterization of intrathecal cerebrospinal fluid geometry and dynamics in cynomolgus monkeys (macaca fascicularis) by magnetic resonance imaging. Plos One. 2019;14(2):e0212239.
27. Smilnak GJ, Charalambous LT, Cutshaw D, Premji AM, Giamberardino CD, Ballard CG, et al. Novel Treatment of Cryptococcal Meningitis via Neurapheresis Therapy. J Infect Dis. 2018;218(7):1147-54.
28. Tangen K, Linninger A, Narasimhan NS. Clearance of subarachnoid hemorrhage from the central nervous system via lumbar drain - a bench-top and computational study. Cerebrovascular Diseases. 2016;41:202-.
29. Steuer H, Jaworski A, Stoll D, Schlosshauer B. In vitro model of the outer blood-retina barrier. Brain Res Brain Res Protoc. 2004;13(1):26-36.
30. Singh NP, Roberts DN. An inexpensive blue filter for fluorescein-assisted repair of cerebrospinal fluid rhinorrhea. Laryngoscope. 2014;124(5):1103-5.
31. Fu BMM, Shen S. Structural mechanisms of acute VEGF effect on microvessel permeability. American Journal of Physiology-Heart and Circulatory Physiology. 2003;284(6):H2124-H35.
32. Kozler P, Pokorny J. Altered blood-brain barrier permeability and its effect on the distribution of Evans blue and sodium fluorescein in the rat brain applied by intracarotid injection. Physiol Res. 2003;52(5):607-14.

33. Sass LR, Khani M, Natividad GC, Tubbs RS, Baledent O, Martin BA. A 3D subject-specific model of the spinal subarachnoid space with anatomically realistic ventral and dorsal spinal cord nerve rootlets. Fluids Barriers CNS. 2017;14(1):36.
34. Fedorow CA, Moon MC, Mutch WAC, Grocott HP. Lumbar Cerebrospinal Fluid Drainage for Thoracoabdominal Aortic Surgery: Rationale and Practical Considerations for Management. Anesthesia and Analgesia. 2010;111(1):46-58.
35. Weaver KD, Wiseman DB, Farber M, Ewend MG, Marston W, Keagy BA. Complications of lumbar drainage after thoracoabdominal aortic aneurysm repair. Journal of Vascular Surgery. 2001;34(4):623-7.
36. Khani M, Sass LR, Xing T, Keith Sharp M, Baledent O, Martin BA. Anthropomorphic Model of Intrathecal Cerebrospinal Fluid Dynamics Within the Spinal Subarachnoid Space: Spinal Cord Nerve Roots Increase Steady-Streaming. J Biomech Eng. 2018;140(8).
37. Tangen K, Narasimhan NS, Sierzega K, Preden T, Alaraj A, Linninger AA. Clearance of Subarachnoid Hemorrhage from the Cerebrospinal Fluid in Computational and In Vitro Models. Ann Biomed Eng. 2016;44(12):3478-94.
38. Gorchynski J, Oman J, Newton T. Interpretation of traumatic lumbar punctures in the setting of possible subarachnoid hemorrhage: who can be safely discharged? Cal J Emerg Med. 2007;8(1):3-7. Epub 2007/02/01.
39. Perry JJ, Alyahya B, Sivilotti MLA, Bullard MJ, Emond M, Sutherland J, et al. Differentiation between traumatic tap and aneurysmal subarachnoid hemorrhage: prospective cohort study. Bmj-Brit Med J. 2015;350.
40. Kuttler A, Dimke T, Kern S, Helmlinger G, Stanski D, Finelli LA. Understanding pharmacokinetics using realistic computational models of fluid dynamics: biosimulation of drug distribution within the CSF space for intrathecal drugs. Journal of Pharmacokinetics and Pharmacodynamics. 2010;37(6):629-44.
41. Keith Sharp M, Carare RO, Martin BA. Dispersion in porous media in oscillatory flow between flat plates: applications to intrathecal, periarterial and paraarterial solute transport in the central nervous system. Fluids and Barriers of the CNS. 2019;16(1):13.
42. Kurtcuoglu V, Soellinger M, Summers P, Poulikakos D, Boesiger P. Mixing and modes of mass transfer in the third cerebral ventricle: a computational analysis. J Biomech Eng. 2007;129(5):695-702.
43. Casalini T, Salvalaglio M, Perale G, Masi M, Cavallotti C. Diffusion and Aggregation of Sodium Fluorescein in Aqueous Solutions. Journal of Physical Chemistry B. 2011;115(44):12896-904.
44. Culbertson CT, Jacobson SC, Michael Ramsey J. Diffusion coefficient measurements in microfluidic devices. Talanta. 2002;56(2):365-73.
45. Longeville S, Stingaciu LR. Hemoglobin diffusion and the dynamics of oxygen capture by red blood cells. Sci Rep. 2017;7(1):10448. Epub 2017/09/07.
46. Khani M, Xing T, Gibbs C, Oshinski JN, Stewart GR, Zeller JR, et al. Nonuniform Moving Boundary Method for Computational Fluid Dynamics Simulation of Intrathecal Cerebrospinal Flow Distribution

in a Cynomolgus Monkey. J Biomech Eng. 2017;139(8):081005.

47. Heidari Pahlavian S, Bunck AC, Thyagaraj S, Giese D, Loth F, Hedderich DM, et al. Accuracy of 4D Flow Measurement of Cerebrospinal Fluid Dynamics in the Cervical Spine: An In Vitro Verification Against Numerical Simulation. Ann Biomed Eng. 2016;44(11):3202-14. Epub 2016/11/04.
48. Levi Chazen J, Dyke JP, Holt RW, Horky L, Pauplis RA, Hesterman JY, et al. Automated segmentation of MR imaging to determine normative central nervous system cerebrospinal fluid volumes in healthy volunteers. Clin Imaging. 2017;43:132-5.
49. Hodel J, Lebret A, Petit E, Leclerc X, Zins M, Vignaud A, et al. Imaging of the entire cerebrospinal fluid volume with a multistation 3D SPACE MR sequence: feasibility study in patients with hydrocephalus. European Radiology. 2013;23(6):1450-8.
50. Courchesne E, Chisum HJ, Townsend J, Cowles A, Covington J, Egaas B, et al. Normal brain development and aging: Quantitative analysis at in vivo MR imaging in healthy volunteers. Radiology. 2000;216(3):672-82.
51. Coffey CE, Lucke JF, Saxton JA, Ratcliff G, Unitas LJ, Billig B, et al. Sex differences in brain aging: A quantitative magnetic resonance imaging study (vol 55, pg 169, 1998). Archives of Neurology. 1998;55(5):627-.
52. Pfefferbaum A, Mathalon DH, Sullivan EV, Rawles JM, Zipursky RB, Lim KO. A quantitative magnetic resonance imaging study of changes in brain morphology from infancy to late adulthood. Arch Neurol. 1994;51(9):874-87.
53. Valen-Sendstad K, Bergersen AW, Shimogonya Y, Goubergrits L, Bruening J, Pallares J, et al. Real-World Variability in the Prediction of Intracranial Aneurysm Wall Shear Stress: The 2015 International Aneurysm CFD Challenge. Cardiovasc Eng Technol. 2018;9(4):544-64.
54. Maeda Y, Shirao S, Yoneda H, Ishihara H, Shinoyama M, Oka F, et al. Comparison of lumbar drainage and external ventricular drainage for clearance of subarachnoid clots after Guglielmi detachable coil embolization for aneurysmal subarachnoid hemorrhage. Clinical Neurology and Neurosurgery. 2013;115(7):965-70.
55. Kwon OY, Kim YJ, Kim YJ, Cho CS, Lee SK, Cho MK. The utility and benefits of external lumbar CSF drainage after endovascular coiling on aneurysmal subarachnoid hemorrhage. Journal of Korean Neurosurgical Society. 2008;43(6):281-7.
56. Hall JE, Guyton AC. Guyton and Hall textbook of medical physiology. 12th ed. Philadelphia, Pa.: Saunders/Elsevier; 2011. xix, 1091 p. p.
57. Riley N. Steady streaming. Annu Rev Fluid Mech. 2001;33:43-65.
58. Sanchez AL, Martinez-Bazan C, Gutierrez-Montes C, Criado-Hidalgo E, Pawlak G, Bradley W, et al. On the bulk motion of the cerebrospinal fluid in the spinal canal. J Fluid Mech. 2018;841:203-27.
59. Tangen KM, Hsu Y, Zhu DC, Linninger AA. CNS wide simulation of flow resistance and drug transport due to spinal microanatomy. J Biomech. 2015;48(10):2144-54.
60. Stockman HW. Effect of anatomical fine structure on the flow of cerebrospinal fluid in the spinal subarachnoid space. J Biomech Eng. 2006;128(1):106-14.

61. Stockman HW. Effect of anatomical fine structure on the dispersion of solutes in the spinal subarachnoid space. J Biomech Eng. 2007;129(5):666-75.
62. Gupta S, Soellinger M, Boesiger P, Poulikakos D, Kurtcuoglu V. Three-dimensional computational modeling of subject-specific cerebrospinal fluid flow in the subarachnoid space. J Biomech Eng. 2009;131(2):021010.
63. Wahlgren NG, Lindquist C. Haem derivatives in the cerebrospinal fluid after intracranial haemorrhage. Eur Neurol. 1987;26(4):216-21.
64. Cruickshank AM. ACP Best Practice No 166: CSF spectrophotometry in the diagnosis of subarachnoid haemorrhage. J Clin Pathol. 2001;54(11):827-30.
65. Defrise M, Gullberg GT. Image reconstruction. Phys Med Biol. 2006;51(13):R139-54. Epub 2006/06/23.
66. Watts R, Steinklein JM, Waldman L, Zhou X, Filippi CG. Measuring Glymphatic Flow in Man Using Quantitative Contrast-Enhanced MRI. AJNR Am J Neuroradiol. 2019;40(4):648-51. Epub 2019/01/27.
67. Sass LR, Khani M, Romm J, Schmid Daners M, McCain K, Freeman T, et al. Non-invasive MRI quantification of cerebrospinal fluid dynamics in amyotrophic lateral sclerosis patients. Fluids Barriers CNS. 2020;17(1):4. Epub 2020/01/22.
68. Menendez Gonzalez M. Implantable Systems for Continuous Liquorpheresis and CSF Replacement. Cureus. 2017;9(2):e1022. Epub 2017/04/18.
69. Baledent O, Gondry-Jouet C, Meyer ME, De Marco G, Le Gars D, Henry-Feugeas MC, et al. Relationship between cerebrospinal fluid and blood dynamics in healthy volunteers and patients with communicating hydrocephalus. Invest Radiol. 2004;39(1):45-55. Epub 2004/01/01.
70. Blitz AM, Shin J, Baledent O, Page G, Bonham LW, Herzka DA, et al. Does Phase-Contrast Imaging through the Cerebral Aqueduct Predict the Outcome of Lumbar CSF Drainage or Shunt Surgery in Patients with Suspected Adult Hydrocephalus? AJNR Am J Neuroradiol. 2018;39(12):2224-30. Epub 2018/11/24.
71. Dreha-Kulaczewski S, Joseph AA, Merboldt KD, Ludwig HC, Gartner J, Frahm J. Inspiration is the major regulator of human CSF flow. J Neurosci. 2015;35(6):2485-91.
72. Takizawa K, Matsumae M, Sunohara S, Yatsushiro S, Kuroda K. Characterization of cardiac- and respiratory-driven cerebrospinal fluid motion based on asynchronous phase-contrast magnetic resonance imaging in volunteers. Fluids Barriers CNS. 2017;14(1):25.
73. Yildiz S, Thyagaraj S, Jin N, Zhong X, Heidari Pahlavian S, Martin BA, et al. Quantifying the influence of respiration and cardiac pulsations on cerebrospinal fluid dynamics using real-time phase-contrast MRI. J Magn Reson Imaging. 2017;46(2):431-9.
74. Pizzichelli G, Kehlet B, Evju O, Martin BA, Rognes ME, Mardal KA, et al. Numerical study of intrathecal drug delivery to a permeable spinal cord: effect of catheter position and angle. Comput Methods Biomech Biomed Engin. 2017:1-10.

Tables

TABLE 1. Mesh details

Parameter	Type
Cell type:	Tetrahedral
Face type:	Triangle
Prism layer:	4
Prism Height:	0.05 (mm)
Growth law:	Exponential
Growth factor:	1.2
Mesh cells:	16.8 M
Mesh faces:	26.4 M
Mesh nodes:	3.7 M
Min mesh size:	0.05 (mm)
Max mesh size:	1.0 (mm)

Time step: 0.1 (s), Cycle: 5th, Time: 100 (s)

TABLE 2. CSF space geometric parameters.

Parameter	Volume (mL)
Spinal cord	19.6
Nerve roots	6.0
Dura	125.9
Total Spinal CSF	**100.3**
Cortical SAS	153.6
Ventricular system	19.7
Cerebellar SAS	21.8
Basal cisterns	26.5
Total Intracranial CSF	**221.6**
Total CSF	*321.9*

Total Spinal CSF = Dura – (Nerve roots + Spinal cord)

Total Intracranial CSF = Cortical SAS + Ventricular system + Cerebellar SAS + Basal cisterns

Figures

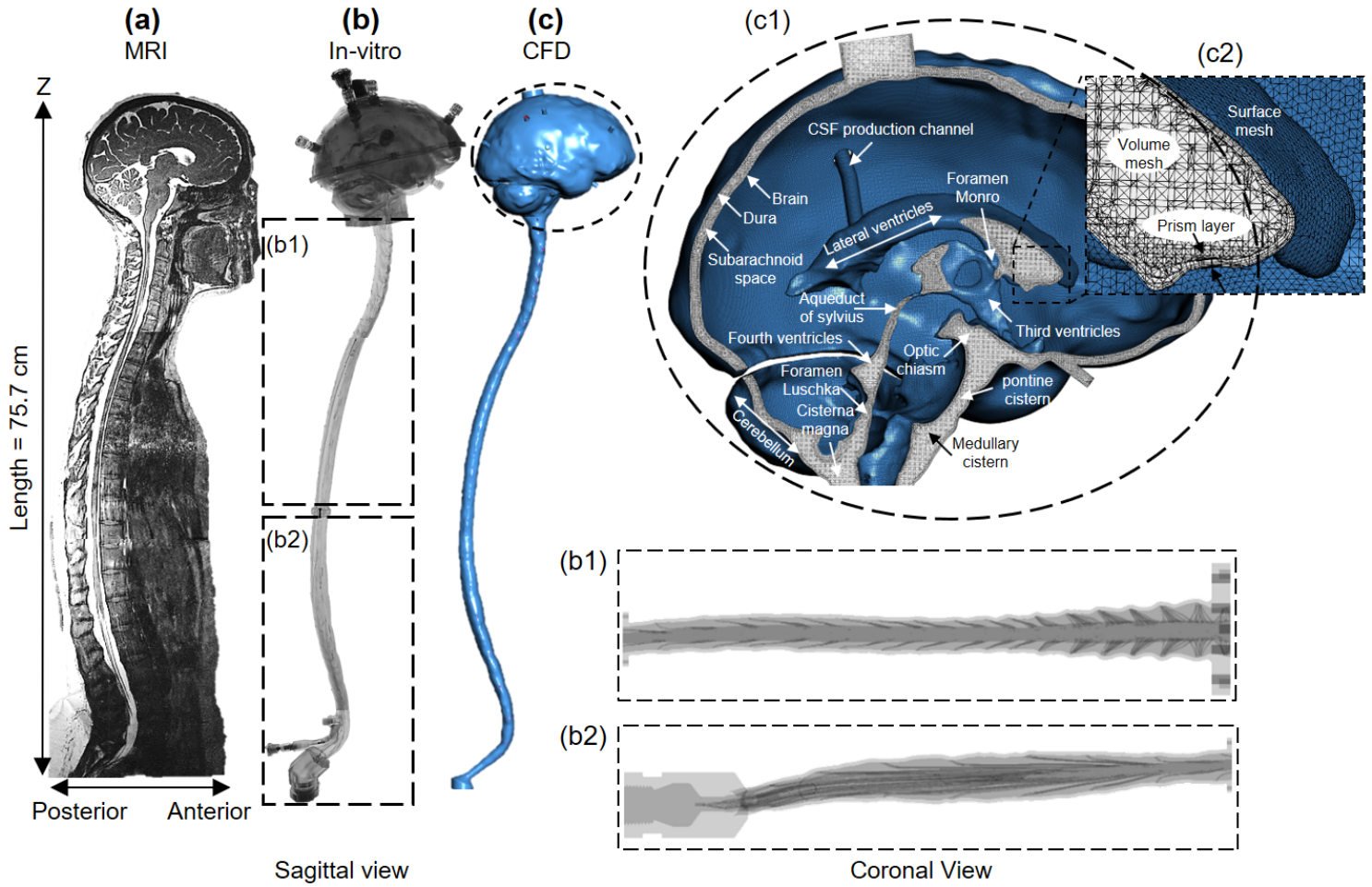

Figure 1

Overview of in vitro and numerical model based on subject specific MRI measurements. (a) T2-weighted MR image of the entire CSF space for the human analyzed to acquire subject-specific anatomy and natural CSF pulsations. (b) An in vitro bench-top model of the human CSF filled spaces was generated from MRI images, (b1-2) In vitro model spinal canal including nerve roots and cauda equina. (c) computational model of the human central nervous system (c1) Magnification of the cranial SAS consisting of lateral ventricles, foramen Monro (left and right), third ventricle, aqueduct of Sylvius, 4th ventricle, foramen Luschka, cisterna magna, pre-pontine and pontine cistern, trigeminal cistern, quadrigeminal cistern, Sylvian cisterns (left and right), and cortical subarachnoid space. (c2) Volumetric and surface mesh visualization with prism layers near the wall.

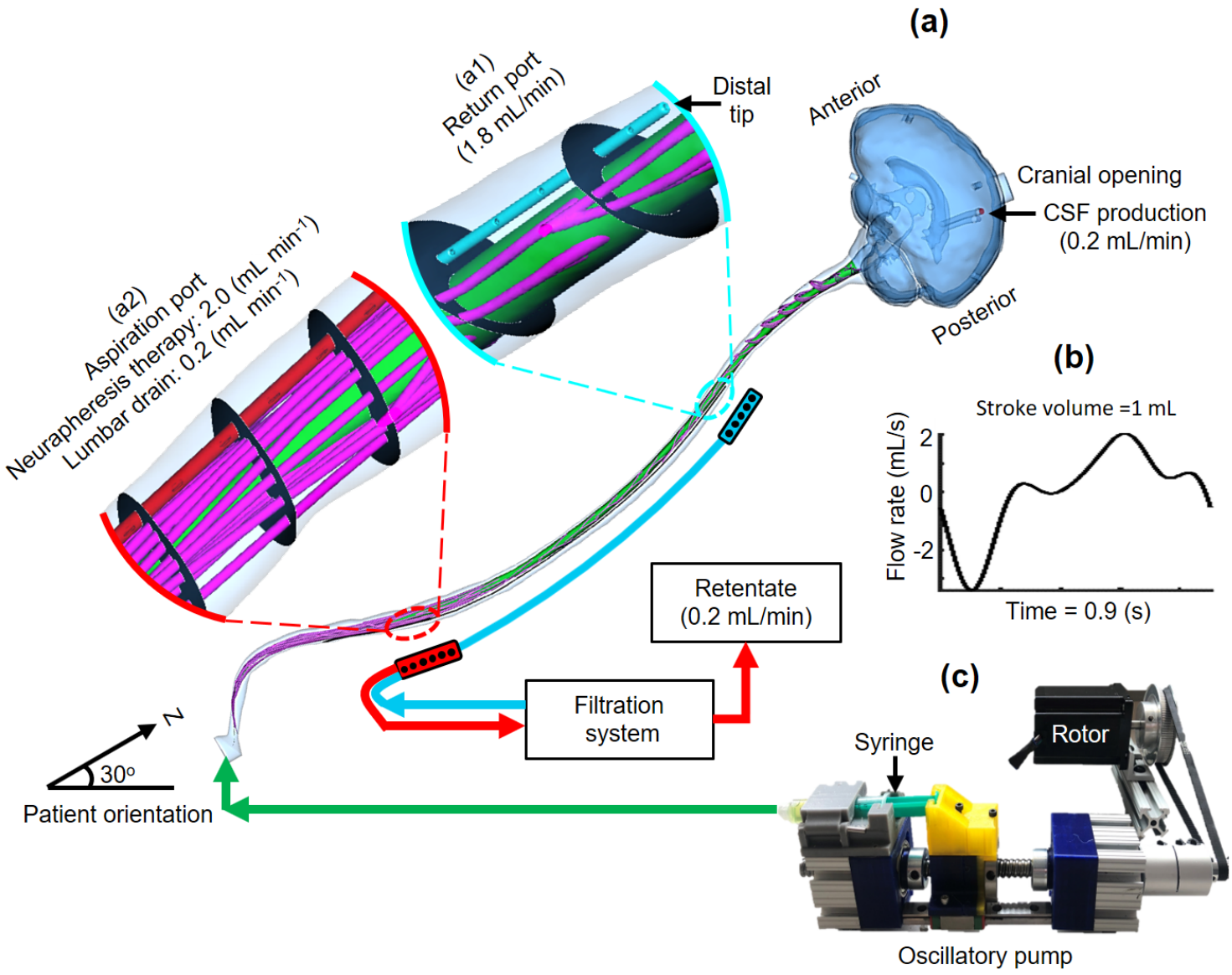

Figure 2

Schematic of the Neurapheresis system and study protocol (a) Three-dimensional CFD model of the SAS with flow boundary conditions and magnified view of the Neurapheresis catheter return and aspiration ports. (b) Oscillatory pump to induce CSF pulsations to match the CSF flow field acquired by phase contrast-MRI.

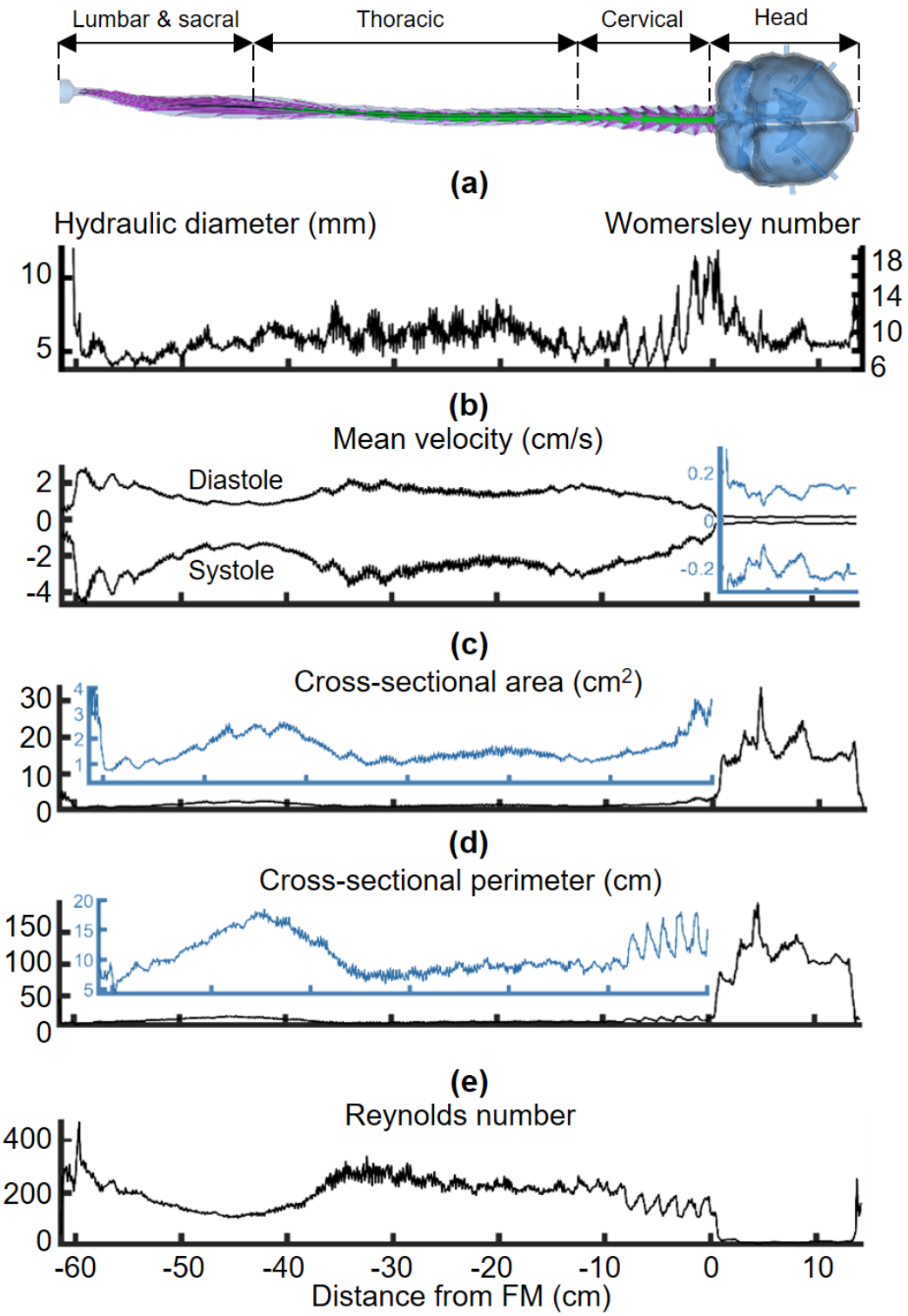

Figure 3

Hydrodynamic and geometric characterization of the computational domain in relation to distance from the foramen magnum (FM). (a) Hydraulic diameter (Left axis) and Womersley number (Right axis), (b) Mean velocity of CSF, (c) cross-sectional area, (d) cross-sectional perimeter of the subarachnoid space, and (e) Reynolds number.

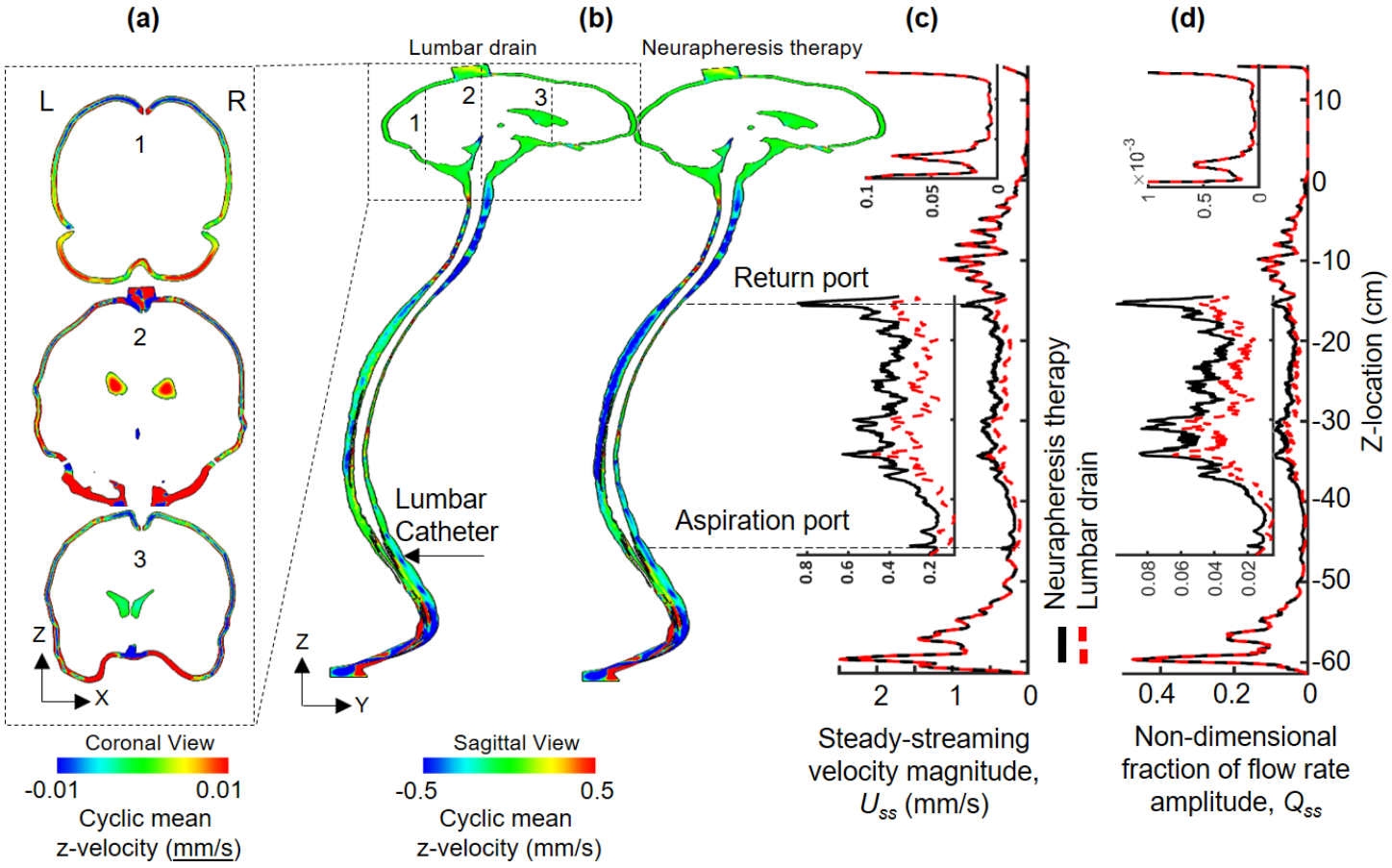

Figure 4

Quantification of steady-streaming velocities. Steady-streaming within the spinal SAS increases with Neurapheresis therapy compared to lumbar drain. (a) Coronal view of cyclic mean z-velocity profiles, , in the cranial SAS is nearly identical for Neurapheresis therapy and lumbar drain. (b) Sagittal view of cyclic mean z-velocity profiles, , simulated by CFD for lumbar drain (left) and Neurapheresis therapy (right). (c) Steady-streaming velocity magnitude, , and (d) non-dimensional fraction of flow rate amplitude, .

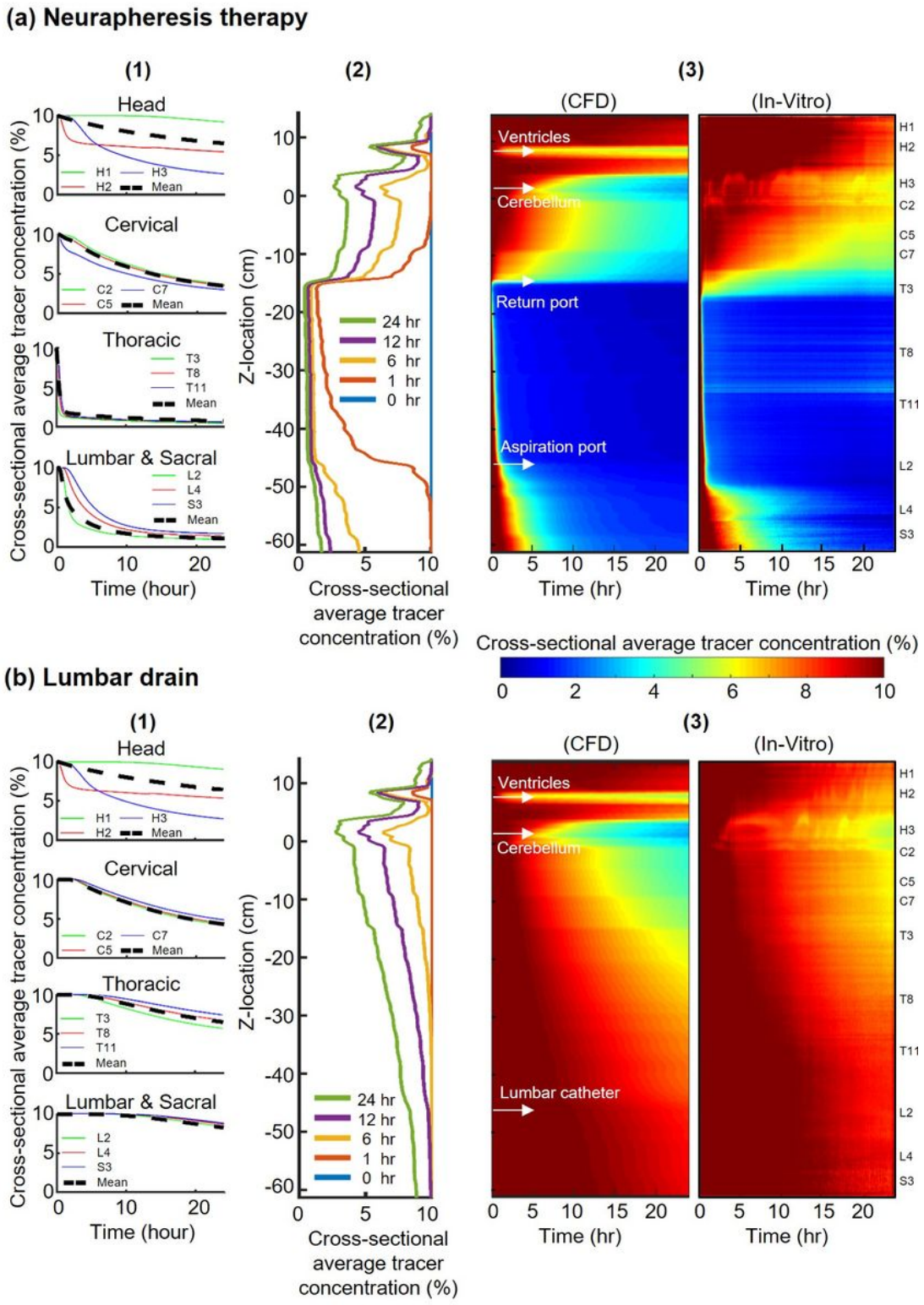

Figure 5

Cross-sectional average tracer concentration over 24-hours. (a) Neurapheresis therapy and (b) lumbar drain. (a1) Cross-sectional average tracer concentration plotted with respect to time at specific axial locations under Neurapheresis therapy. (a2) Cross-sectional average tracer concentration along the neuroaxis for different time points, t= 0, 1, 6, 12, and 24 hours under Neurapheresis therapy. (a3) spatial temporal plot for cross-sectional average tracer concentration for CFD and in-vitro under Neurapheresis

therapy along the model for 24-hours. (b1) Cross-sectional average tracer concentration plotted with respect to time at specific axial locations under lumbar drain. (b2) Average tracer concentration along the neuroaxis for different time points, t=0, 1, 6, 12, and 24 hours under lumbar drain. (b3) spatial temporal plot for cross-sectional average tracer concentration for CFD and in-vitro under lumbar drain along the model for 24-hours.

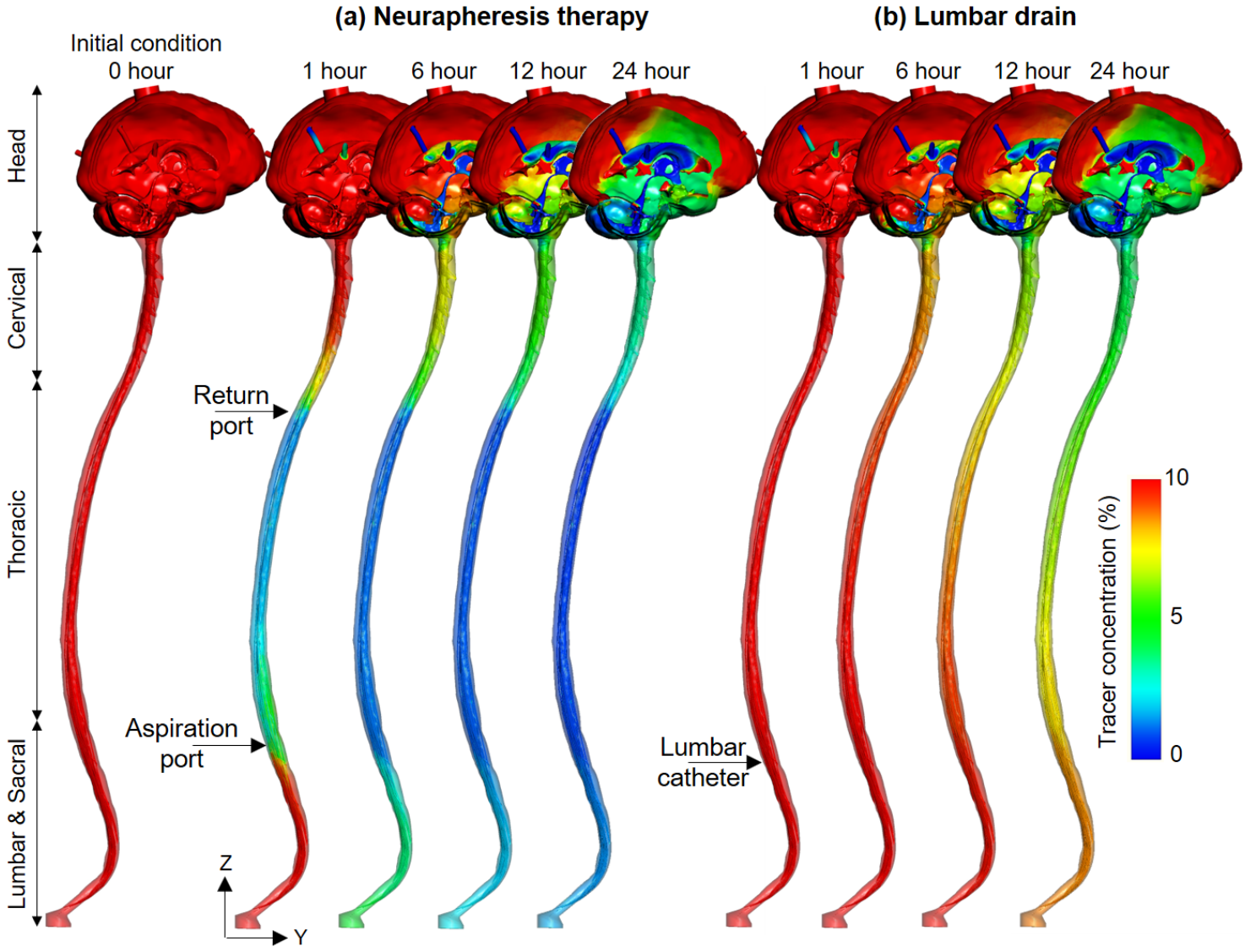

Figure 6

CFD results for 2D tracer concentration profiles versus time under Neurapheresis therapy and lumbar drain. (a) Visualization of tracer concentration at 0, 1, 6, 12, and 24 hours under Neurapheresis therapy, and (b) Visualization of tracer concentration at 1, 6, 12, and 24 hours under lumbar drain.

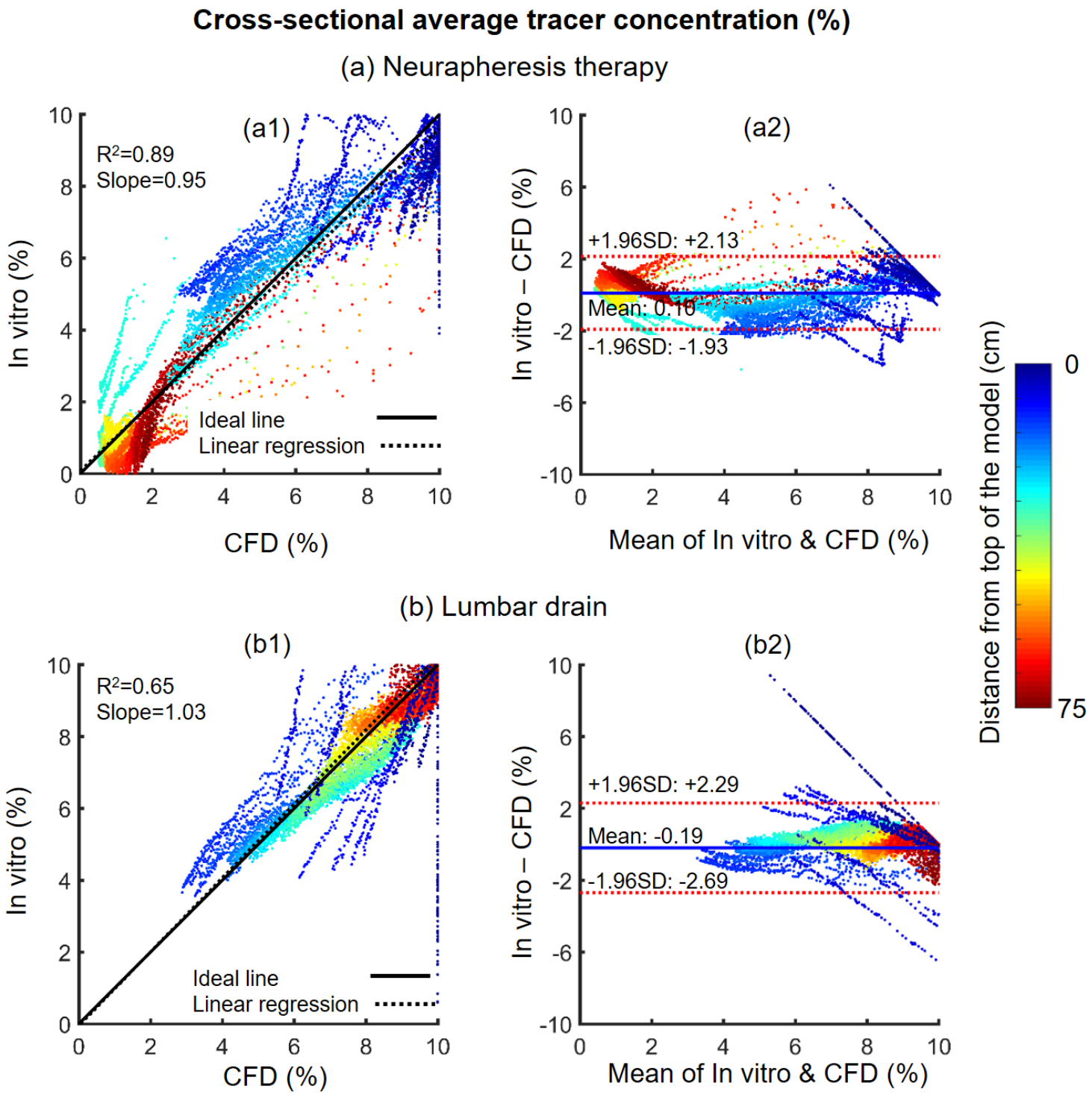

Figure 7

Correlation and Bland-Altman plots for agreement of in vitro and numerical simulation results for spatial-temporal cross-sectional average tracer concentration over 24-hours. (a) Neurapheresis therapy and (b) lumbar drain. The linear regression is shown in black dashed line (left subplots, a1 and b1) and the limit of agreement (95% confidence intervals) lines are shown in dashed lines (right subplots, a2 and b2).

Supplementary Files

This is a list of supplementary files associated with this preprint. Click to download.

- Results.docx
- Methods.docx